npj | Materials Degradation

www.nature.com/npjmatdeg

ARTICLE OPEN

Check for updates

Influence of high heating rates on evolution of oxides on directed laser energy additively fabricated IN718

Sangram Mazumder[1], Mangesh V. Pantawane[1] and Narendra B. Dahotre[1]✉

The effect of non-isothermal treatment in oxygen-containing air, via heating rates of 10, 50, and 1000 °C/min until 1000 °C followed by furnace cooling to room temperature on oxides formed on directed laser energy additively fabricated IN718 was studied. Another set of samples heated up to 1000 °C using the same heating rates were isothermally held at 1000 °C for 1 hr followed by furnace cooling to room temperature. X-ray photoelectron spectroscopy indicated the presence of NiO on samples only heated at 1000 °C/min. Also, results indicated the absence of Fe-oxides on non-isothermally treated samples, irrespective of heating rate. However, isothermal treatment confirmed the presence of NiO on all samples and Fe-oxides on samples heated via 50 and 1000 °C/min. The durations in complement with the kinetics of the thermal treatments influenced oxide evolution in the samples. Such an experimental approach was adopted to study the material response under dynamic short duration-high temperature oxidation.

npj Materials Degradation (2021)5:45 ; https://doi.org/10.1038/s41529-021-00193-2

INTRODUCTION

Laser-based directed energy deposition (L-DED) is a widely used additive manufacturing (AM) technique capable of creating free-standing 3-dimensional (3D) structures and coating/cladding an existing metallic component[1,2]. With this technique, a nickel-based superalloy-IN718 is amongst easily fabricable alloys due to its superior weldability and availability in the form of powder/wire feedstock[3,4]. The combination of high-temperature mechanical properties and resistance to high-temperature oxidation of IN718 make them highly desirable for applications in energy and aerospace applications[5,6]. The presence of Ni and Cr in IN718 provides excellent resistance to oxidation at high temperatures owing to the nature of their oxide films.

The investigation of the oxidation process often follows conventional methodologies involving isothermal treatment in the temperature range of 700–1000 °C for extended hours which allows determining oxidation behavior (linear, parabolic, and logarithmic) exhibited by these samples[7–10]. While the majority of these isothermal high temperature oxidation experiments are performed using a heating rate of 10 °C/min—a commonly used heating rate, it is often far from any heating rates associated with the initial stages of practical high-temperature applications[11]. This is because, high-temperature applications such as aerospace engines and thruster components experience a sudden rise in temperature through extremely steep thermal gradients due to combustion in the engine, thereby experiencing high heating rates during the initial stages of their operations followed by a long duration near stabilized high-temperature combustion. Hence, it is important to consider the thermokinetic aspects associated with such high-temperature service environments by conducting oxidation studies adopting high heating rates. Such an approach is likely to help in identifying the morphologies and stoichiometries of nucleating oxides which in turn may influence the evolution of types of oxides (morphology and stoichiometry) in a long-duration oxidation process. Even though initial transient stages of oxidation are governed by the thermodynamics of the process, the following long-duration oxidation is predominantly governed by diffusion of the constituent species. Hence, it is challenging to identify any thin oxidation layers for their transitionary physical and chemical evolutions after long-duration oxidation.

Hence, in the present study, a two-prong approach of heat treatment for oxidation of L-DED fabricated IN718 was adopted. In one set of experiments involved high heating rate non-isothermal treatment whereas another set of experiments involved high heating rate non-isothermal treatment followed by high-temperature isothermal treatment. Such approach of heat treatment (details are provided below) was followed with the aims and objectives (1) to identify the stoichiometries nucleated during non-isotherm treatments and (2) to study the effects of the oxides nucleated as a template during non-isothermal treatment on the evolution of the oxide stoichiometries during follow up isothermal treatment. On the contrary, during conventional oxidation studies basically, the samples are isothermally soaked at high temperatures for longer durations of time (several hours).

These two approaches on thermal treatments are obviously associated with totally different thermokinectics and hence likely to result in different combinations of oxidation stoichiometries and their morphologies and evolution sequence.

In light of this, the present study was focused on the thermal treatment of L-DED fabricated IN718 in oxygen-containing synthetic air, via heating rates of 10, 50, and 1000 °C/min until 1000 °C followed by either furnace cooling for non-isothermal treatment or holding at 1000 °C for 1 h and then furnace cooling for isothermal treatment. The oxidation characteristics of the L-DED fabricated IN718 samples were studied from the thermo-gravimetric analysis (TGA) plots obtained during heat treatment and the oxidized samples were characterized for the oxide product stoichiometry using X-ray photoelectron spectroscopy (XPS).

It is extremely difficult to resolve the complex transient modes associated with the evolution of multiple oxides on both temporal and spatial basis using any experimental technique. In view of this, the development of a gradual understanding based on

[1]Laboratory for Laser Aided Additive and Subtractive Manufacturing, Department of Materials Science and Engineering, Center for Agile and Adaptive Additive Manufacturing, University of North Texas, Denton, TX, USA. ✉email: Narendra.Dahotre@unt.edu

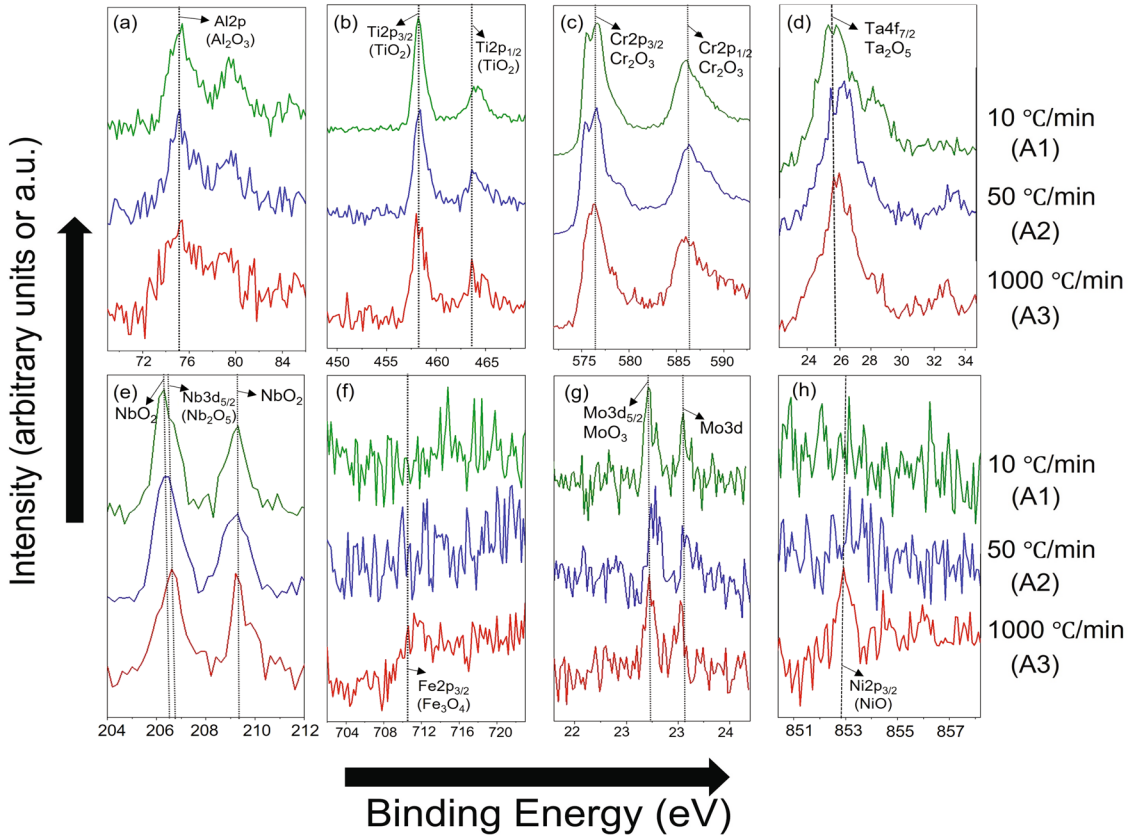

Fig. 1 XPS spectral analysis of non-isothermally treated L-DED fabricated IN718. Spectra corresponding to the component elements **a** Al, **b** Ti, **c** Cr, **d** Ta, **e** Nb, **f** Fe, **g** Mo, and **h** Ni.

fundamental scientific principles was considered a sound foundation. The preliminary efforts presented in the current paper remain the foundation for ongoing study for gaining an in-depth understanding of morphological and crystallographic evolution of these oxide species, parallel efforts are ongoing for an in-depth understanding of morphological and crystallographic evolutions of these oxide species and their thorough characterization by employing the high-resolution electron microscopy techniques such as scanning transmission electron microscopy (STEM), transmission electron microscopy (TEM), and atom probe tomography (APT). The outcome of these efforts will be reported in future publications.

RESULTS AND DISCUSSION

Non-isothermal oxidation

High-resolution XPS analysis of non-isothermally treated L-DED fabricated IN718 samples detected the peaks corresponding to the oxides of Al, Ti, Cr, Ta, Nb, Fe, Mo, and Ni (Fig. 1). While the peaks of oxides of Al, Ti, Cr, Ta, Nb, and Mo were prominent and sharp at all heating rates, the oxide peaks of Ni were barely detectable at commonly used (10 °C/min, sample A1) and higher (50 °C/min, sample A2) heating rates and became noticeable at the heating rate of 1000 °C/min (sample A3) (Fig. 1h), and oxide peaks corresponding to Fe oxides remained barely noticeable, irrespective of the heating rates (Fig. 1f). Also, the presence of oxides of Al, Ti, Cr, Ta, Nb, and Mo on samples from group A (A1–A3) indicated that variations in heating rates in a high-temperature oxidative environment had conceivably marginal or no effect on the formation (particularly in stoichiometry) of these oxides on the L-DED fabricated IN718 samples (Fig. 1a–e, g). In fact, the presence of chromia (Cr_2O_3); an oxide on which superalloys like IN718 depend for high-temperature oxidation resistance[12], on L-DED fabricated IN718, indicated that it was apparently capable of maintaining its high-temperature oxidation resistance(at 1000 °C) even under extremely rapid heating condition (1000 °C/min) (sample A3, Fig. 1c).

The oxide formation is driven by the thermodynamic force which can be recognized from the Gibbs free energy change, ΔG values associated with the formation of a given oxide. The formation of a given oxide among others is favored based on the extent of their ΔG changes associated with the formation of that oxide at a particular temperature[13]. The change in ΔG associated with the oxides of the constituent elements of IN718 (Al_2O_3, TiO_2, Cr_2O_3, Ta_2O_5, Nb_2O_5, NbO_2, $FeO/Fe_3O_4/Fe_2O_3$, MoO_3, and NiO) as a function of temperature are presented in Fig. 2[14–16]. The nucleation followed by the lateral growth of these oxides is likely to follow the order influenced by the factors such as kinetics and temperature, availability of the reactive species at the reaction site, and diffusion rate of reacting species. In the present study, the kinetics of oxidation appeared to become crucial in the lateral growth of oxides during non-isothermal treatment. The non-isothermal treatment at heating rates of 10 °C/min and 50 °C/min until 1000 °C spanned over a maximum of 75 and 20 min, respectively (refer to "Methods and materials" section). The time involved in such high-temperature treatment appeared to be enough for the thermodynamically more-favorable oxides (Al_2O_3, TiO_2, Cr_2O_3, Ta_2O_5, Nb_2O_5, NbO_2, $FeO/Fe_3O_4/Fe_2O_3$, and MoO_3) to predominantly grow over the thermodynamically less-favorable ones (NiO), as observed in samples A1 and A2 (Fig. 1h). On the contrary, as the non-isothermal treatment at a heating rate of 1000 °C/min until 1000 °C spanned over only 1 minute, the presence of thermodynamically more-favorable oxides (Al_2O_3, TiO_2, Cr_2O_3, Ta_2O_5, Nb_2O_5, NbO_2, $FeO/Fe_3O_4/Fe_2O_3$, and MoO_3) along with nucleation of NiO were detected in sample A3 (Fig. 1h).

TGA curves representing the change in mass (%) with time for samples A1 and A2 (Fig. 3a, b) clearly indicated that the samples A1 and A2 just started gaining mass after an initial drop (marked by red arrows) which can be attributed to the removal of moisture and/or other impurities within the sample followed by the occurrence of early stages of oxidation[17]. On the contrary, in sample A3, heated at 1000 °C/min, the heat treatment time is significantly short (1 min), oxides of the elements other than Ni failed to predominantly grow over NiO (Fig. 1h). Accordingly, due to the lack of any recognizable oxidation and related mass gain in sample A3, the slope of the TGA curve remained negative over the entire non-isothermal treatment (Fig. 3c). Furthermore, the TGA analysis also clearly indicated that during the mass gain phases of the non-isothermal treatments of samples A1 and A2 (Fig. 3a, b), along with oxides of all elements of IN718, the rapid and extensive formation of thermodynamically favorable Cr_2O_3 (Fig. 2) (also due to significantly high Cr content of 17.0 wt%) predominantly grown over nuclei of NiO thereby indicating the absence of XPS peaks corresponding to NiO (Fig. 1h).

Although oxidation of Fe (FeO and Fe_3O_4) below ~450° is thermodynamically more favorable than that of Mo (Fig. 2), XPS peaks corresponding to Fe-oxides were absent (Fig. 1f) but that corresponding to Mo-oxides present (Fig. 1g), in all three samples A1–A3. This can be attributed to the relatively lower diffusion coefficient (4.8×10^{-112} cm^2/s)[18] associated with Fe diffusion through Fe oxides, discussed later in this study. Hence, even though Fe oxidation into FeO and Fe_3O_4 below ~450 °C is thermodynamically favorable (Fig. 2), it was thermokinetically very sluggish. Therefore, the formation of a minor amount of Fe oxides through such sluggish reactions in the sample set A remained undetectable within the instrumental detection limits of XPS (Fig. 1f). Moreover, the oxides of other elemental components of IN718 including but not limited to Al, Ti, Cr, Nb, also competitively outgrew small amounts of Fe oxides due to the sluggish growth rate associated with Fe oxides. A significant amount of Cr (17.0 wt %), along with 0.75 wt% Ti and 0.3 wt% Al, in the L-DED fabricated IN718 ensured the rapid lateral growth of chromia (Cr_2O_3), and also, titania (TiO_2) and alumina (Al_2O_3) with high thermodynamic driving forces associated with their formation compared to the formation of all oxides of other elements in the alloy (Fig. 1), throughout the surface with the possibilities of predominantly growing over whatever minor quantity of oxides of both, Fe and Ni were formed.

Previously, it was showed that in an alloy AB, the minimum weight concentration of C_B of element B essential for the formation of a continuous external layer can be calculated by the equation[19]

$$C_B = \frac{V}{Z_B M_O} \frac{\pi \times K_p}{(D)} \frac{1}{2} \quad (1)$$

where V is the molar volume of the alloy, Z_B is the valency of B atoms, M_O is the atomic weight of oxygen, K_p is the parabolic rate constant for B_2O_{ZB} formation, and D is the diffusion coefficient of element B in AB alloy. Using Eq. 1, Wright et al. estimated the values for C_B for Ni–Cr system, and the calculations revealed that Cr concentration within 12.3–18.0 wt% was capable of forming a continuous external Cr_2O_3 layer[20]. In light of this, a 17.0 wt% of Cr in IN718 was expected to form a continuous external Cr_2O_3 layer to predominantly grow over the thermodynamically less favorable oxides of Ni and Fe that were evolved in relatively minor quantities. Furthermore, although evaporation of Cr/Cr_2O_3 at high temperatures (>900 °C) has been previously reported, such evaporation was appeared to be recognizable only after long exposure times (100–1000 h) at these temperatures[21–23]. In light of this, in the present dynamic non-isotherm oxidation study, involving extremely short duration (1–160 min) up to 1000 °C, the evaporation of Cr, even if occurred, was not likely to occur in a recognizable amount.

Finally, similar to the presence of NiO in short duration non-isothermal treatment (1000 °C/min until 1000 °C) of sample A3, the presence of strong NiO electron diffraction lines in early stages of oxidation prior to the establishment of a healing Al-rich (γ-Al_2O_3) layer in a Ni–Al system was also previously confirmed by Chattopadhyay et al.[24]. In the same report, it was mentioned that this particular phenomenon also holds for Ni–Cr system, except the healing (formation of Cr_2O_3) was a little less rapid. Moreover, once nucleated, the growth of NiO at early stages of oxidation, appeared to occur more rapidly due to relatively high diffusion coefficients associated with Ni in NiO (6.2×10^{-4} cm^2/s) and/or in NiO (9.13×10^{-9} cm^2/s), (Table 1), despite the fact that another

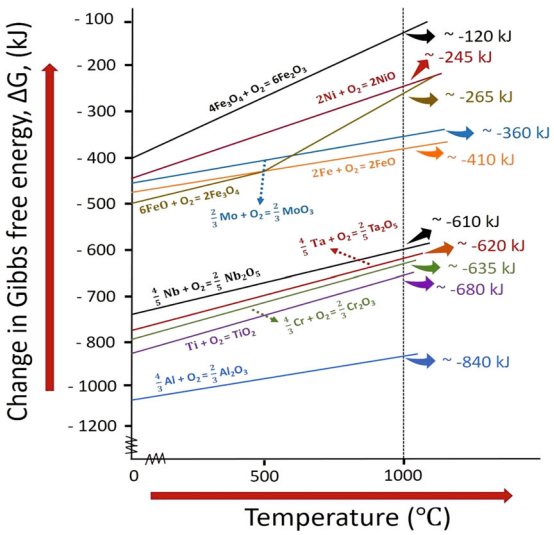

Fig. 2 Ellingham diagram for metals. Ellingham diagram for the oxidation reactions of metallic constituents of IN718[14–16].

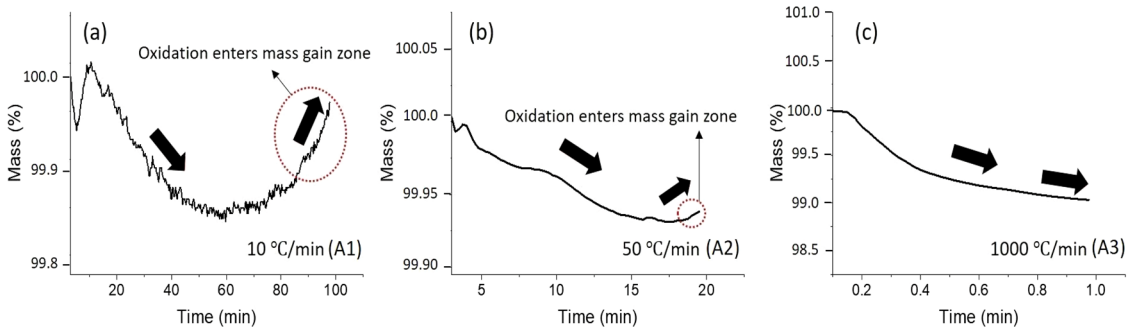

Fig. 3 TGA analysis for change in mass with time of non-isothermally treated L-DED fabricated IN718. TGA plots correspond to heating rates of **a** 10 °C/min, **b** 50 °C/min, and **c** 1000 °C/min.

oxide like Cr_2O_3 is thermodynamically more favored. The XPS evaluation (Fig. 1g) indicated that the growth kinetics of NiO dominated over the growth kinetics of other oxides at high heating rates. This mechanism in complement with larger content of Ni (50 wt.%) allowed the growth of NiO in the uncovered regions of the surface left by the other oxides. Thus especially, the rapid and shorter time thermal treatment of sample A3 prevented other more stable and thermodynamically preferable oxides (Al_2O_3, TiO_2, Cr_2O_3, Ta_2O_5, Nb_2O_5, NbO_2, $FeO/Fe_3O_4/Fe_2O_3$, and MoO_3) from predominantly growing over Ni oxide. This occurrence can be attributed to the absence of Ni oxide (NiO) peaks on A1 and A2 samples whereas the presence of NiO on sample A3 (Fig. 1h). Thus, it was clear that in the non-isothermally treated samples, with the increase in the heating rate, the samples possessed distinct templates of the oxides of various constituent elements based on their proportions.

Table 1. Diffusion modes of constituent elements of IN718 and corresponding diffusion coefficients[19,25,28,30,31,33–35].

Diffusion Mode of Constituent Elements in IN718	Diffusion Coefficient (cm^2/s)
Oxygen in Cr_2O_3	5.2×10^{-15} [33]
Oxygen in MoO_3	$2.7 \pm 0.75 \times 10^{-3}$ [34]
Oxygen in Nb_2O_5	1.72×10^{-2} [28]
Oxygen in TiO_2	1.2×10^{-15} [28]
Oxygen in Nio	9.13×10^{-9} [30]
Oxygen in Ta_2O_5	8.6×10^{-7} [30]
Ni in Nio	6.2×10^{-4} [31]
Cr in Cr_2O_3	4.8×10^{-18} [35]
Al in Al_2O_3	1.65×10^{-18} [35]
Fe in Fe_2O_3	4.8×10^{-112} [35]

Isothermal oxidation

The XPS surface analysis of the isothermally treated set of samples (B) clearly indicated the presence of distinctly resolved and sharp peaks of various oxides: Al_2O_3, TiO_2, Cr_2O_3, Ta_2O_5, Nb_2O_5, NbO_2, $FeO/Fe_3O_4/Fe_2O_3$, and MoO_3 and NiO (Fig. 4). These oxides appeared to have grown from the previously evolved (nucleated) oxides during the initial non-isothermal stage of this (isothermal) treatment, similar to that in the treatment of the A set of samples (Fig. 2). Here, the effect of the oxide template evolved during earlier non-isothermal treatment can be noticed on the subsequently grown oxides. The presence of relatively high proportions of $FeO/Fe_3O_4/Fe_2O_3$ (Fig. 4f) produced in samples B2 and B3, and NiO (Fig. 4h) produced in sample B3 seemed to favor the formation of the recognizable quantity of these oxides during isothermal treatment compared to that formed during non-isothermal treatment (set of samples A, Fig. 1f, h).

There are two theories often used to describe the formation of passive oxide films on metals during oxidation. The Cabrera–Mott theory holds for thin films at room temperature and the Wagner oxidation theory is used in the case of thicker oxide layers[25,26]. Both these models propose that the growth of an oxide film results from the motion of cation or anion vacancies in presence of an electric field and can be helpful in explaining the evolution of oxides in the present study. Diffusion of either oxygen through the metal oxide to the metal oxide–metal interface, or diffusion of metal ion through the metal oxide to the metal oxide–atmosphere interface is considered as the key step for growth/thickening of metal oxide layers. Hence, any impedance or admittance to these pathways will clearly influence the reaction kinetics in overriding thermodynamical aspects in imparting sluggishness to an otherwise spontaneous reaction. Thus, although the above-mentioned phenomenon may prevail during metal oxide growth, for oxide

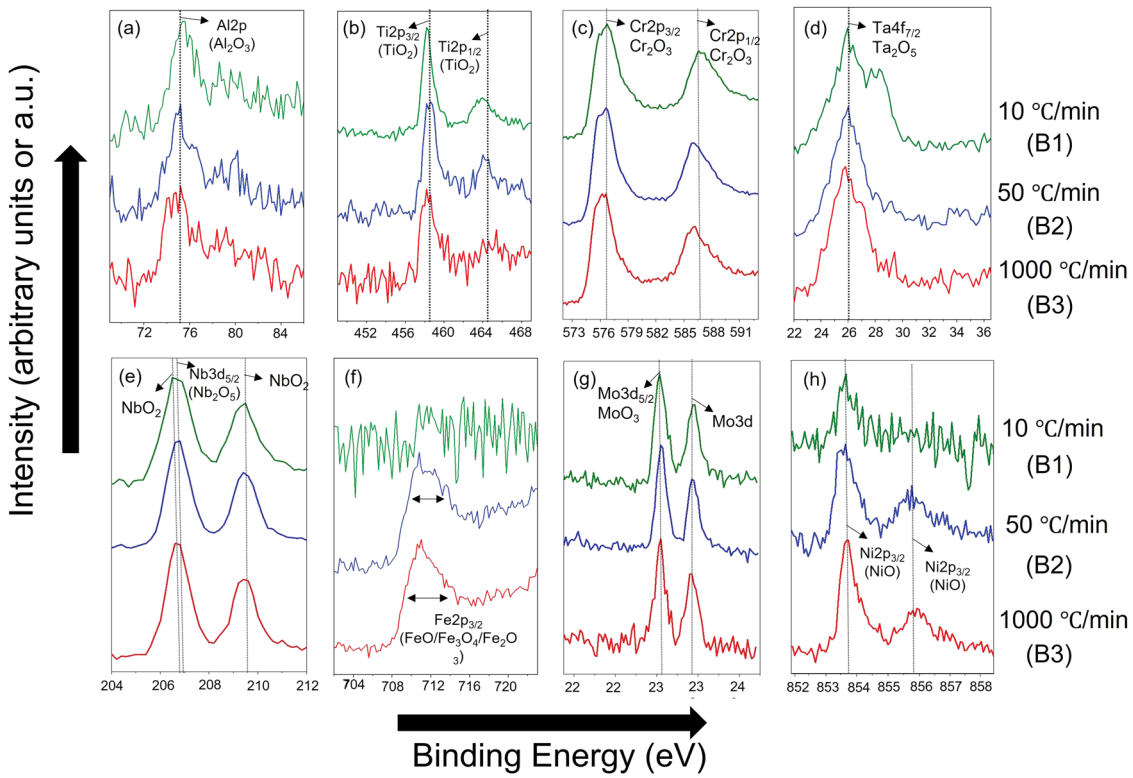

Fig. 4 XPS spectral analysis of isothermally treated L-DED fabricated IN718. Spectra corresponding to the component elements **a** Al, **b** Ti, **c** Cr, **d** Ta, **e** Nb, **f** Fe, **g** Mo, and **h** Ni.

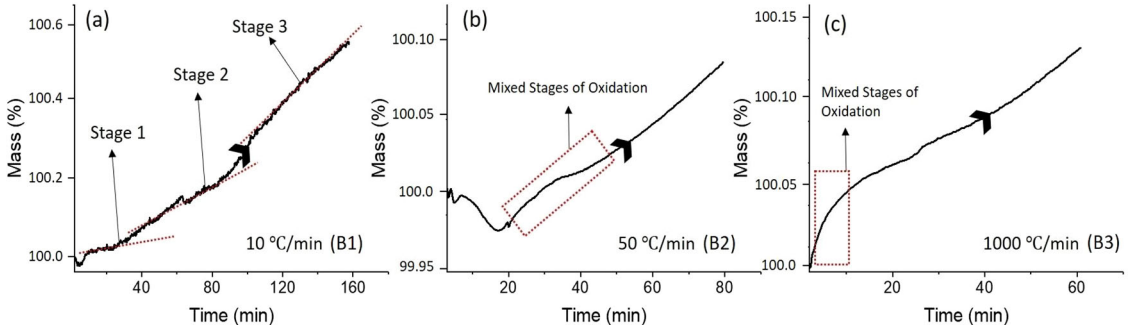

Fig. 5 TGA analysis for change in mass with a time of isothermally treated L-DED fabricated IN718. TGA plots correspond to heating rates of **a** 10 °C/min, **b** 50 °C/min, and **c** 1000 °C/min.

nucleation, thermodynamics of the reaction(s) is more crucial provided there existed an ample amount of reactive species. Sabioni et al. recently reported the bulk and grain boundary diffusion of oxygen in both single and polycrystalline Cr_2O_3 in a temperature range of 1000–1450 °C, which showed greater oxygen diffusion coefficients, compared to that of Cr[27]. Similarly, oxygen diffusion was also favored over Nb diffusion through Nb_2O_5 and Ta diffusion through Ta_2O_5, owing to the higher mobility of oxygen compared to Nb and Ta in their respective oxides[28,29]. On the contrary, the diffusion coefficient of oxygen (9.13×10^{-9} cm^2/s) is lower than that of Ni (6.2×10^{-4} cm^2/s) in NiO (Table 1)[30,31]. However, in this study, the extremely less exposure period (especially for non-isothermally treated sample A3) of the L-DED fabricated IN718 in a high-temperature oxidative environment was most likely to have produced very thin oxide layers (less than 1000 Å), as indicated by the XPS peak intensities (Fig. 1h, sample A3). As mentioned by Jeangros et al.[32] the initial thin NiO layer growth was qualitatively related to the description of Cabrera–Mott model according to which, once the NiO domains are impinged, oxide growth commences by field-driven transport of Ni^{2+} through NiO. Although, once each elemental oxides are nucleated, they experienced growth by the virtue of either cationic or anionic or even both movements through the oxide layers during the isothermal holding of the L-DED fabricated IN718 samples at 1000 °C for 1 h.

In addition, 50.0 wt% of Ni content of IN718 significantly helped in the nucleation and growth of NiO while the growths of oxides of other elements were limited by their relatively lower concentration. This phenomenon further clarifies the presence of distinct NiO peaks in isothermally oxidized all samples of set B (B1–B3) of IN718 (Fig. 4h). Although NiO peaks were visibly absent in XPS spectra corresponding to non-isothermally treated A1 and A2 samples (Fig. 1h), their nucleation and presence (even if in minute amounts) may not be ignored because these nuclei have further helped the growth of a significant amount of NiO during isothermal treatment of B1, and B2 samples (Fig. 4h). Hence, the 1 h isothermal hold at 1000 °C resulted in rapid growth and proliferation of the NiO on all oxidized L-DED fabricated IN718 samples. Similarly, the oxidation of Fe proceeds via cationic transport through the oxide layer which facilitates Fe ions to travel to the metal oxide atmosphere interface where the growth of the oxide layer takes place. The diffusion coefficient of Fe in Fe_2O_3 was reported to be 4×10^{-112} cm^2/s, over a range of 750–1000 °C (Table 1)[18]. Despite the sluggish reaction kinetics of Fe oxidation reaction, 1 h isothermal treatment was apparently long enough for the evolution of Fe-oxides in samples B2 and B3 enough to be detected by XPS analyses (Fig. 4f). However, it should also be considered that along with Fe all other constituent elements of IN718, were exposed all together, at high temperatures for a longer time (2 h 40 min). Extended exposure times at high temperatures beyond a certain limit can in turn influence the oxidation kinetics of every element, strongly enough to predominantly grow over the slow-growing Fe oxides. Hence, in such cases, the relatively higher oxidation kinetics of other elements in IN718 can lead to the rapid growth of other oxides and this may have resulted in XPS spectra with undetected Fe oxides peaks, even after long exposure times at high-temperature conditions (sample B1, Fig. 4f). This phenomenon further explains the absence of XPS peaks corresponding to Fe oxides in sample B1 but, presence of the same in samples B2 and B3.

TGA curves for sample set B (Fig. 5) indicated that all samples (B1–B3) entered the recognizable mass gain zone which was due to long duration (1 h), high temperature (1000 °C) isothermal treatment. Sample B1 clearly indicates the classic three-stage oxidation of IN718 (Fig. 5a)[17], where, in stage 1 oxidation is comparatively less in terms of mass gain, in stage 2 there is steady-state oxidation and finally in stage 3, there is rapid oxidation (mass gain). The presence or absence and duration of these oxidation stages appeared to be characteristic of the non-isothermal heating rate prior to isothermal heat treatment of L-DED fabricated IN718 (Fig. 5). With increasing heating rate, the initial stages of oxidation appeared to be mixed together or undefined at the beginning which then directly proceeded to the third stage of rapid oxidation zone and this third stage continued till the end of the isothermal treatment (Fig. 5b, c). Hence, the distinctly characteristic three-stage oxidation process changed to two-stage (bimodal) or single-stage (single mode) oxidation with increasing heating rates from 10 to 1000 °C/min. The TGA curve representing a heating rate of 10 °C/min is associated with three distinct stages of oxidation (Fig. 5a) and that representing 1000 °C/min lacks clear distinction and appeared to be mixed together (Fig. 5c) whereas the TGA curve for 50 °C/min represents two-stage oxidation process (Fig. 5b).

While thermodynamics sets the near-equilibrium path for the oxidation process, it is a kinetics that plays a pivotal role in determining the evolution of oxide species. In actual service, the heating rates are often higher than considered in the previous oxidation studies reported in the open literature. Therefore, in the present study, it was reasonable to consider the non-isothermal treatment involving rapid heating rates followed by isothermal treatment at a higher temperature to evaluate the growth of oxide species. In the present study, attempts were made to clearly indicate the significance of the kinetics of thermal treatment through the dominance of growth of Ni-oxides and Fe-oxides over other oxides during certain stages of oxidation. Even for an element like Ni that has the lowest thermodynamic driving force (ΔG) a rapid non-isothermal treatment (1000 °C/min at up to 1000 °C) nucleated detectable amount of Ni oxide and even though Fe experiences a relatively slow (sluggish) oxidation reaction kinetics, an isothermal hold for 1 h at 1000 °C facilitated the growth of Fe oxides. The template of different proportions of such oxides produced on the surface during non-isothermal

Table 2. Laser processing parameters used during L-DED fabrication of IN718.

Power (W)	Speed (mm/s)	Laser beam diameter (mm)	Laser track overlap (mm)	Laser beam residence time (s)	Laser fluence (J/mm^2)
350	5.83	1	0.65	0.17	79

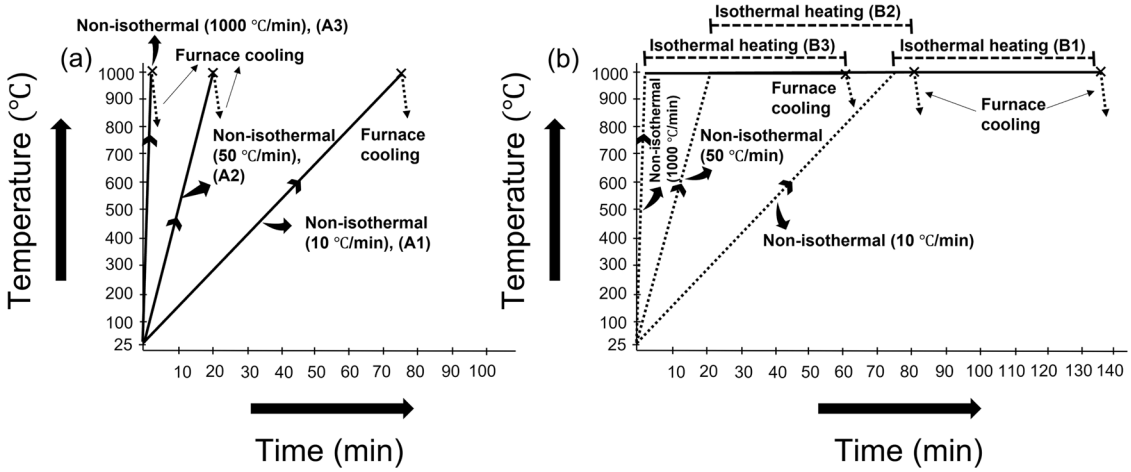

Fig. 6 Schematic of oxidation thermal treatments of L-DED fabricated IN718. a Non-isothermal oxidation with heating rates of 10 °C/min (A1), 50 °C/min (A2), and 1000 °C/min (A3) until 1000 °C followed by furnace cooling to room temperature (23 °C), and **b** isothermal oxidation with heating rates of 10 °C/min (B1), 50 °C/min (B2), and 1000 °C/min (B3) until 1000 °C followed by isothermally holding at 1000 °C for 1 h and then furnace cooling to room temperature (23 °C).

oxidation treatment eventually governed the growth and, in turn, their proportion after the isothermal treatment. In summary, the major outcomes of this study include the following points:

1. Non-isothermal treatments of L-DED fabricated IN718 resulted in the oxidation of Al, Ti, Cr, Ta, Nb, and Mo at all the three heating rates of 10, 50, and 1000 °C/min until 1000 °C. However, the XPS analysis indicated the presence of Ni oxides in the sample heated at 1000 °C/min, while oxidation of Fe was not detected at any employed heating rates.
2. The isothermal treatments after each non-isothermal heating led to further oxidation of all elements, including Ni and Fe, as detected by XPS. However, the kinetically-assisted effect enhanced the oxidation of Ni and Fe, which was recognized in the isothermal treatment preceded by high heating rates (50 and 1000 °C/min).
3. With increasing heating rate, three distinct stages of mass gain during IN718 oxidation appeared to be distinct only in the case of isothermal treatment using the lowest heating rate (10 °C/min). In the case of higher heating rates (50 and 1000 °C/min), the initial stages of oxidation were relatively undefined which then directly proceeded to the third oxidation stage of rapid mass gain.

As the present study was focused on the preliminary characterization of the oxidation behavior of AM fabricated IN718, it extensively employed XPS analysis of the evolution of oxide stoichiometries during non-isothermal treatment as well as the effect of these oxides templates developed during non-isothermal treatment on the further evolution of stoichiometries in follow up isothermal treatment. However, this being an ongoing study for gaining an in-depth understanding of morphological and crystallographic evolution of these oxide species, parallel efforts are ongoing on the thorough characterization of these oxides by employing high-resolution electron microscopy including but not limited to STEM, TEM, and APT that are intended to be reported in future publications.

METHODS

Powder

Commercially available Ar atomized powder of superalloy Inconel® 718 (UNS N07718) as per ASTM F3055 specifications was obtained from Carpenter Technology and used for producing AM samples using L-DED. The average composition of the major elements in the powder included 50.0 Nickel, 17.0 Chromium, 4.75 Niobium and Tantalum, 2.2 Molybdenum, 0.75 Titanium, 0.3 Aluminum, and balance Iron; all in wt%. Powder particle size was in the range of 45 and 105 µm.

L-DED process

L-DED was carried out using a Hybrid Manufacturing Technology Ambit Mini Mill system equipped with an Nd:YAG laser (1.06 µm wavelength) of 1200 W capacity. The laser beam was associated with a Gaussian energy distribution (TEM_{00} mode). Laser beam diameter was 1 mm on the sample surface, whereas, a laser beam overlap of 0.6 mm was implemented to ensure complete consolidation of the deposited samples. Laser beam rastering velocity was maintained at 5.83 mm/s which led to a laser beam residence time of 0.17 s, expressed as the ratio between laser beam diameter and laser rastering velocity. A laser fluence of 79 J/mm^2 was calculated from Eq. 2, based on the present set of laser processing parameters (Table 2).

$$\text{Laser Fluence} = \frac{\text{Laser Power} \times \text{Laser Beam Residence Time}}{\text{Laser Beam Cross} - \text{sectional Area on Sample Surface}} \quad (2)$$

These laser processing parameters were selected for L-DED fabrication of IN718 in the present study based on the extensive background and experience in laser-material interaction and laser-based processing and manufacturing of the current research group. Furthermore, these parameters were carefully chosen to fabricate a physically sound sample devoid of any physical defects within the sample (porosity, cracks, etc.).

In the present work L-DED based AM for IN718 was considered due to several general characteristics associated with the technique that are but not limited to (1) higher deposition rates at relatively low resolution leading to faster build rate, (2) since the precursor material is fed during the process on demand from separate powder containers process can be controlled less wastage and feed rates to control the thermokinetics of the process, (3) creates higher density parts with better mechanical properties, (4) produces near net shapes requiring minimal amount of post-processing, (5) highly suited for repairing applications, and (6) comparably larger parts can be built.

Table 3. Description of types of oxidation thermal treatments of L-DED fabricated IN718 and designation of corresponding sample groups.

Sample group	Sample name	Oxidation treatment (at 1000 °C in 20–22 vol% O_2 in air)	Designation of oxidation treatment
A	A1	Oxidation with a heating rate of 10 °C/min until 1000 °C followed by furnace cooling to room temperature (23 °C)	Non-isothermal oxidation
	A2	Oxidation with a heating rate of 50 °C/min until 1000 °C followed by furnace cooling to room temperature (23 °C)	
	A3	Oxidation with a heating rate of 1000 °C/min until 1000 °C followed by furnace cooling to room temperature (23 °C °C)	
B	B1	Oxidation with a heating rate of 10 °C/min until 1000 °C followed by holding at 1000 °C for 1 h and then furnace cooling to room temperature (23 °C)	Isothermal oxidation
	B2	Oxidation with a heating rate of 50 °C/min until 1000 °C followed by holding at 1000 °C for 1 h and then furnace cooling to room temperature (23 °C)	
	B3	Oxidation with a heating rate of 1000 °C/min until 1000 °C followed by holding at 1000 °C for 1 h and then furnace cooling to room temperature (23 °C)	

Oxidation experiment and XPS characterization

A total of six samples measuring 4 × 4 × 4 mm were sectioned out from the L-DED fabricated IN718 components using Struers Secotom-60. The average weight of these samples prior to oxidation studies was 0.21 mg. Oxidation of these L-DED fabricated IN718 samples was carried out using Netzsch, STA 449 F3 Jupiter TGA equipped with a high heating rate (up to 1250 °C/min) furnace. The samples were oxidized in the air (ultra-zero certified grade) containing 20–22 vol% of oxygen, purchased from Matheson Tri-Gas Inc. The sectioned IN718 samples were split into two groups: A and B.

The high-temperature oxidation of the L-DED fabricated IN718 was conducted in oxygen-containing air, adopting a two-prong approach. One set of samples were subjected to non-isothermal treatment via heating rates of 10, 50, and 1000 °C/min until 1000 °C followed by furnace cooling to room temperature (group A) whereas the second set of samples was subjected to the thermal treatment via high heating rates of 10, 50, and 1000 °C until 1000 °C and isothermally held at that temperature for 1 h followed by furnace cooling to room temperature (group B). These thermal treatments are schematically illustrated with various details in Fig. 6 and summarized in Table 3. These non-isothermal and non-isothermal plus isothermal treatments adopted in this present study were intended to seek qualitative insight into oxidation similar to high-temperature applications such as aerospace engines and thruster components.

After oxidation of the L-DED fabricated IN718 samples, the oxide products were detected using XPS. XPS investigations were performed using a PHI 5000 Vesaprobe scanning XPS instrument. The binding energy data were referenced to the aliphatic C 1 s peak at 284.4 eV. The oxidized samples were transferred into the XPS chamber right after the furnace was cooled down to room temperature (23 °C), without allowing any significant seating time in between the oxidation experiments and XPS analyses, thus preventing oxide product evolution after the experimental regime, at room temperature.

DATA AVAILABILITY

Data supporting the findings of this study are available from the corresponding author and the first author upon reasonable request.

Received: 2 June 2021; Accepted: 13 August 2021;
Published online: 01 September 2021

REFERENCES

1. Gibson, I., Rosen, D. & Stucker, B. Directed energy deposition processes. in *Additive Manufacturing Technologies*. 245–268 (Springer, 2015).
2. Saboori, A. et al. Application of directed energy deposition-based additive manufacturing in repair. *Appl. Sci.* **9**, 3316 (2019).
3. Pantawane, M. V. et al. Spatial variation of thermokinetics and associated microstructural evolution in laser surface engineered in718: Precursor to additive manufacturing. *Metall. Mater. Trans. A* **52**, 1–17 (2021).
4. Jinoop, A. N., Paul, C. P., Mishra, S. K. & Bindra, K. S. Laser additive manufacturing using directed energy deposition of Inconel-718 wall structures with tailored characteristics. *Vacuum* **166**, 270–278 (2019).
5. Zhai, Y., Lados, D. A., Brown, E. J. & Vigilante, G. N. Understanding the microstructure and mechanical properties of ti-6al-4v and Inconel 718 alloys manufactured by laser engineered net shaping. *Addit. Manuf.* **27**, 334–344 (2019).
6. Sui, S. et al. Laves phase tuning for enhancing high temperature mechanical property improvement in laser directed energy deposited Inconel 718. *Compos. B Eng.* **215**, 108819 (2021).
7. Luo, G. et al. Preferential interdendritic oxidation of laser additively manufactured Inconel 718. *Corros. Sci.* **179**, 109144 (2021).
8. Jia, Q. & Gu, D. Selective laser melting additive manufactured Inconel 718 superalloy parts: high-temperature oxidation property and its mechanisms. *Opt. Laser Technol.* **62**, 161–171 (2014).
9. Juillet, C., Oudriss, A., Balmain, J., Feaugas, X. & Pedraza, F. Characterization and oxidation resistance of additive manufactured and forged in 718 Ni-based superalloys. *Corros. Sci.* **142**, 266–276 (2018).
10. Kang, Y. J., Yang, S., Kim, Y. K., AlMangour, B. & Lee, K. A. Effect of post-treatment on the microstructure and high-temperature oxidation behavior of additively manufactured Inconel 718 alloy. *Corros. Sci.* **158**, 108082 (2019).
11. Bruce Cassel, R. *High Heating Rate Dsc*. 297. (TA Instruments Technical Publication, TA, 2002).
12. Pint, B. A., Dryepondt, S. & Unocic, K. A. Oxidation of superalloys in extreme environments. in *Proc. 7th International Symposium on Superalloy 718 and Derivatives*. 861–875. (TMS-AIME Warrendale, PA, 2010).
13. Birks, N., Meier, G. H. & Pettit, F. S. *Introduction to the High Temperature Oxidation of Metals*. (Cambridge University Press, 2006).
14. Hasegawa, M. Ellingham diagram. in *Treatise on Process Metallurgy*. 507–516 (Elsevier, 2014).
15. Saji, V. S. & Lopatin, S. I. *Molybdenum and its Compounds: Applications, Electrochemical Properties and Geological Implications*. (Nova Science Publishers, Inc., 2014).
16. Osaki, S., Sakai, H. & Suzuki, R. O. Direct production of ti–29nb–13ta–4.6 Zr biomedical alloy from oxide mixture in molten $CaCl_2$. *J. Electrochem. Soc.* **157**, E117 (2010).
17. Nath, S., Manna, I. & Dutta Majumdar, J. Compositionally graded thermal barrier coating by hybrid thermal spraying route and its non-isothermal oxidation behavior. *J. Therm. Spray. Technol.* **22**, 901–917 (2013).
18. Himmel, L., Mehl, R. F. & Birchenall, C. E. Self-diffusion of iron in iron oxides and the Wagner theory of oxidation. *JOM* **5**, 827–843 (1953).
19. Wallwork, G. R. The oxidation of alloys. *Rep. Prog. Phys.* **39**, 401 (1976).
20. Stringer, J. & Wright, I. G. The high-temperature oxidation of cobalt-21 wt.% chromium-3 vol.% y 2 o 3 alloys. *Oxid. Met.* **5**, 59–84 (1972).
21. Falk-Windisch, H., Svensson, J. E. & Froitzheim, J. The effect of temperature on chromium vaporization and oxide scale growth on interconnect steels for solid oxide fuel cells. *J. Power* **287**, 25–35 (2015).
22. Sachitanand, R., Sattari, M., Svensson, J. E. & Froitzheim, J. Evaluation of the oxidation and cr evaporation properties of selected FeCr alloys used as SOFC interconnects. *Int. J. Hydrog. Energy* **38**, 15328–15334 (2013).
23. Yamauchi, A., Kurokawa, K. & Takahashi, H. Evaporation of Cr_2O_3 in atmospheres containing H_2O. *Oxid. Met.* **59**, 517–527 (2003).
24. Wood, G. C. & Chattopadhyay, B. Transient oxidation of ni-base alloys. *Corros. Sci.* **10**, 471–480 (1970).

25. Cabrera, N. F. M. N. & Mott, N. F. Theory of the oxidation of metals. *Rep. Prog. Phys.* **12**, 163–184 (1949).
26. Atkinson, A. Wagner theory and short circuit diffusion. *Mater. Sci. Technol.* **4**, 1046–1051 (1988).
27. Sabioni, A. C. S., Huntz, A. M., Millot, F. & Monty, C. Self-diffusion in Cr_2O_3 III. Chromium and oxygen grain-boundary diffusion in polycrystals. *Philos. Mag. A* **66**, 361–374 (1992).
28. Chen, W. K. & Jackson, R. A. Diffusion of oxygen in near-stoichiometric α-Nb_2O_5. *J. Chem. Phys.* **47**, 1144–1148 (1967).
29. Nakamura, R. et al. Diffusion of oxygen in amorphous Al_2O_3, Ta_2O_5, and Nb_2O_5. *J. Appl. Phys.* **116**, 033504 (2014).
30. Perusin, S., Monceau, D. & Andrieu, E. Investigations on the diffusion of oxygen in nickel at 1000 c by sims analysis. *J. Electrochem. Soc.* **152**, E390 (2005).
31. Hallwig, D., Sockel, H. G. & Monty, C. Oxygen diffusion in NiO and ZnO. in *Reactivity of Solids*, 631–634 (Springer, 1977).
32. Jeangros, Q. et al. Oxidation mechanism of nickel particles studied in an environmental transmission electron microscope. *Acta Mater.* **67**, 362–372 (2014).
33. Tsai, S. C., Huntz, A. M. & Dolin, C. Growth mechanism of cr2o3 scales: oxygen and chromium diffusion, oxidation kinetics and effect of yttrium. *Mater. Sci. Eng. A* **212**, 6–13 (1996).
34. St Clair, T. P., Restad, J. M. & Ted Oyama, S. Oxygen diffusivity in moo 3 as determined by a temperature programmed method. *J. Mater. Res.* **13**, 1430–1433 (1998).
35. Sabioni, A. C. S., Huntz, A. M., Philibert, J., Lesage, B. & Monty, C. Relation between the oxidation growth rate of chromia scales and self-diffusion in Cr_2O_3. *J. Mater. Sci.* **27**, 4782–4790 (1992).

ACKNOWLEDGEMENTS

The authors acknowledge the infrastructure and support of the Center for Agile & Adaptive Additive Manufacturing (CAAAM) funded through State of Texas Appropriation #190405-105-805008-220 at the University of North Texas (UNT). The authors also acknowledge the availability of the analytical facility for this work in the Materials Research Facility (MRF) at UNT.

AUTHOR CONTRIBUTIONS

The authors S.M., M.V.P., and N.B.D. conceived the presented idea. S.M. designed and performed the experimental work. S.M. wrote the paper with significant consultation support from M.V.P. and N.B.D. N.B.D. reviewed and advised the whole work.

COMPETING INTERESTS

The authors declare no competing interests.

ADDITIONAL INFORMATION

Correspondence and requests for materials should be addressed to N.B.D.

Reprints and permission information is available at http://www.nature.com/reprints

Publisher's note Springer Nature remains neutral with regard to jurisdictional claims in published maps and institutional affiliations.